

## Improved calculation of Si sputter yield via first principles derived interatomic potential

M.Z. Hossain<sup>a,\*</sup>, J.B. Freund<sup>a,b</sup>, H.T. Johnson<sup>a</sup>

<sup>a</sup> Department of Mechanical Science and Engineering, University of Illinois at Urbana-Champaign, IL 61801, USA

<sup>b</sup> Department of Aerospace Engineering, University of Illinois at Urbana-Champaign, IL 61801, USA

### ARTICLE INFO

#### Article history:

Received 15 December 2008

Received in revised form 26 January 2009

Available online 5 February 2009

#### PACS:

34.20.Cf

34.35.+a

68.49.Sf

79.20.-m

#### Keywords:

Interatomic potential

Density functional theory

Sputter yield

### ABSTRACT

Silicon sputter yield under medium energy Ar<sup>+</sup> ion bombardment is calculated via molecular dynamics, using a highly accurate interatomic potential for Ar–Si interactions derived from first-principles calculations. Unlike the widely used universal repulsive potentials such as the Moliere or ZBL parameterizations, this new potential, referred to as DFT–ArSi, is developed via localized basis density functional theory. Sputter yields for Si obtained with the DFT–ArSi potential at 500 eV and 1 keV incident energies are found to be within 6% and 2% of experimental results, respectively, while errors using existing potentials are typically on the order of 11%. The DFT–ArSi potential differs from existing empirical potentials in the ~1 Å interatomic separation range which is shown to be the most important range for modeling low-to-medium energy ion bombardment.

© 2009 Elsevier B.V. All rights reserved.

### 1. Introduction

Sputtering, whereby atoms are ejected from target material due to ion bombardment, is used for various processes such as film deposition, etching, or for analysis in Secondary Ion Mass Spectroscopy (SIMS). Silicon is one of the most important and widely used semiconductor materials; it is also well understood atomistically and many highly accurate interatomic potentials are available. However, despite these factors, the mechanisms of silicon sputtering are not well understood theoretically or computationally. Bridging this gap, by focusing on the interatomic model for Ar–Si interactions, is the objective of the present work.

Sputtering is usually measured experimentally. Among the reported experimental results, there are some observed discrepancies in the literature. A few experimental results that were performed prior to 1965 and compiled by Wittmaack [1], show unusually low sputter yields for Si. However, Zalm [2] address the reliability of these older experiments and compile a larger number of experimental results and more recent data. Silicon sputter yield is the focus of this article; it is found to be 0.88 for 1 keV Ar<sup>+</sup> bombardment and 0.63 for 500 eV Ar<sup>+</sup> bombardment. In com-

putational studies of ion bombardment of Si, sputter yields are readily attainable, yet most available computational studies show significantly lower yields than are reported in experiments, especially at lower bombardment energies.

Interatomic potentials are the foundation for the dynamical time-stepping process in molecular dynamics simulations and correspondingly, the outcomes of MD studies may be strongly affected by the choice of potentials. Stansfield et al. [3] show a strong influence of empirical potentials e.g. Smith potential, Moliere potential and Universal potential on the results of sputter yields in MD simulations. The Ar–Si system is often modeled by empirical potentials such as the Moliere or ZBL potentials [4,5], or by other potentials among those studied by Stansfield et al. All of these potentials predict Si sputter yields much different from experimental findings. The ZBL potential that is often used to determine sputter yields for different materials using the Monte Carlo algorithm underestimates the results by a factor of 2 or more especially at lower ion impact energies. Using the software package SRIM [6], which uses the ZBL potential, Shulga [7] compute Si sputter yield to be 0.72 for 1 keV Ar-ion bombardment on Si, which deviates by 23% from the experimental value of 0.93. The 500 eV Si sputter yield is computed to be 0.45 – more than 25% less than the experimental value of 0.63. At the same energy Stansfield et al. [3] compute Si sputter yield to be 0.70 with the SCF potential and 0.84 with Smith potential. These widely used potentials are typically obtained by

\* Corresponding author.

E-mail address: [zubaexy@gmail.com](mailto:zubaexy@gmail.com) (M.Z. Hossain).

fitting exponential functions to limited experimental data or by averaging hundreds of computed screening functions for various pair interactions, from which general conclusions are made for a wide range of atom pairs. While these empirical potentials have the advantage of providing some level of universality, none represent Ar–Si interactions with sufficient accuracy to model sputtering.

The choice of interatomic potential can yield different values for other calculated properties for ion bombardment, such as the stopping power at low energy, but there is no clear guidance to help select the most appropriate potential for a particular atom-ion pair [8]. Stansfield et al. [3] note that different potential functions better describe atom interactions in different energy ranges. The influence of ion-atom potentials is also discussed by Harrison [9], Webb and Harrison [10], Shapiro and Lu [11], Schuller et al. [12], García and Miraglia [13] and the usefulness of creating or modifying empirical interatomic potentials using quantum-mechanical calculations is demonstrated by several other groups [14–21]. A specific atom-pair potential is shown to estimate penetration angle better than the ZBL or Moliere potentials; Using new potentials, developed by *ab initio* methods, Stansfield et al. [3,15] show an improved estimate for sputter yields for Ar<sup>+</sup>–Cu(001) and classically computed trajectories for Ar–Si(001). Given the sensitivity and the relatively extreme energies of the ion impacts, it is expected that the accuracy of such simulations will also benefit from a more fundamental description of the interactions.

In developing empirical potentials such as those described above, there is generally some attempt to account for electrostatic or electronic structure effects, though not at the level of first-principles. In the development of the Moliere potential for example, a few properties determined in classical experiments for a wide variety of atom pairs are averaged and fitted to a sum of three exponential functions that model the repulsive energetic interactions between a pair of atoms of any two species. This procedure is expected to yield a potential that represents the general trends, but not the particular details of any specific atom pairs. In another approach, Ziegler et al. [5] (ZBL) evaluate screening functions for 261 different atom pairs assuming each of the two atoms, in a pair, to have a spherically symmetric charge distribution with a central point charge. In this case, the Thomas–Fermi screening length is adjusted to reproduce the shape of the implant profile. To generalize the potential a suitable reduced radial coordinate is introduced and the computed screening functions are contracted by arbitrarily imposing a screening length. This procedure neglects correlation effects, electrons are assumed to be confined to a spatially limited cell and no spatial distortion of the electron clouds is taken into consideration. These approximations are expected to be less accurate at close separation distances. In the present work, we employ density functional theory [22] which accounts for these factors and develop a potential specifically for Ar–Si interactions including the effect of neighboring Si atoms. The analysis incorporates an accurate quantum mechanical description of interactions between the atoms. The new potential is found to much more accurately predict sputter yield for the Ar–Si system than existing empirical potentials. Also, because it is based upon an accurate fundamental calculation, it is expected to be accurate over a broader energy range of application than existing empirical potentials.

## 2. Methodology

An approach to compute sputter yield using molecular dynamics is described in detail in previous articles [23,24] and is summarized briefly here. To compute Si sputter yield, a target of 8000 Silicon atoms is prepared with 10 repeated 8-atom unit cells of crystalline Si in each of the three coordinate directions. The lattice

constant of Si is taken as 0.5431 nm. Periodic boundary conditions are enforced in the [010] and [010] directions and an Ar<sup>+</sup> ion is sent from vacuum toward the [001] surface. Throughout the dynamic simulations the atoms in the bottom layer of the simulation domain are held stationary while the rest of the system is integrated in time using the velocity-Verlet algorithm with a time step of 0.15 fs. The time step is sufficient to track atomic interactions accurately in an MD simulation of the Ar–Si system at low energy ion bombardment [23].

At the beginning of the simulation, before sending the ion toward the target, a Berendsen thermostat is applied to all atoms to equilibrate the target to an average thermal energy corresponding to 77 K. The Ar<sup>+</sup> projectile ion is then directed normal to the [001] surface at a random position on the initially crystalline Si target; the projectile has a kinetic energy of either 500 eV or 1 keV depending on the simulation case. Si sputter yield, defined as the number of Si atoms leaving the [001] surface per Ar<sup>+</sup> impact, is computed by tracking the number of target atoms that escape the Si surface after the impact and traveling more than a distance of 1.5 nm normal to the surface; these atoms never return to the surface and in all cases this occurs within 2.25 ps of the impact, for either 500 eV or 1 keV incidence energies. At the first ion impact the instantaneous sputter yield is very low since the target is crystalline. With more ion impacts the average sputter yield gradually increases and a steady-state is obtained after around 20 impacts on the target domain, which corresponds to a fluence level of about 1.5E14 ions/cm<sup>2</sup>. This fluence has been shown to be sufficient for obtaining a converged sputter yield result at both 500 eV and 700 eV Ar<sup>+</sup> bombardment of a Si [001] surface [23]. By the time this fluence is achieved, the crystallinity of the Si target is lost; the semiconductor surface is, in fact, amorphized quite easily at fairly low Ar<sup>+</sup> fluences [25,26]. For each choice of the impact energy, converged sputter yield results are determined as arithmetic averages over five different values of statistical parameter in the calculation that assigns initial thermal velocities to the target atoms randomly, assuring that the molecular dynamics results are properly ensemble averaged. Indeed, no significant variation is observed with averaging of additional cases.

The molecular dynamics calculation requires interatomic potential models for Ar–Si repulsive interactions and Si–Si covalent interactions. For Si–Si interactions there are several potentials available in the literature, most of which are optimized for the crystalline phase of Si. The Stillinger–Weber (SW) potential [27], however, was developed with both the solid and liquid phases of Si in mind. This potential is shown to be the best choice for modeling Si–Si interactions in cases involving a large amount of disorder and defects [3]. Sputtering that involves significant surface damage created by the ion impacts can thus be modeled with the SW potential. For Ar–Si interactions, which are mainly repulsive in nature, no potential is available in the literature that has been developed specifically for the Ar–Si pair. Here a localized basis density functional theory is used to derive the Ar–Si potential. The potential, referred to as DFT–ArSi, is used to obtain the Si sputter yield.

### 2.1. Ar–Si interactions using a first-principle based potential

To obtain a potential for Ar–Si interactions based on first-principles electronic structure, the SIESTA [28] (Spanish Initiative for Electronic Simulations with Thousands of Atoms) implementation of self-consistent density functional theory is used, where an *ab initio* calculation is performed with norm conserving pseudopotentials and a flexible linear combination of numerical atomic orbitals (NAOs) basis. The core electrons are replaced by Troullier–Martins pseudopotentials [29] and valence electrons are described by a double-zeta, polarized orbitals basis set.

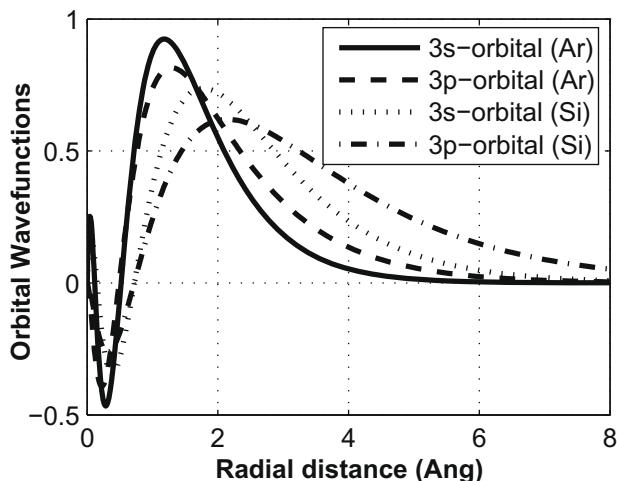


**Fig. 1.** All-electron wavefunctions of atomic orbitals for Si and Ar. The outermost node is formed at  $\sim 0.5$  a.u. for Ar and at  $\sim 0.7$  a.u. for Si.

Pseudopotentials for Ar and Si are first generated with electronic configurations of  $1s^2 2s^2 2p^6 3s^2 3p^6 3d^0 4f^0$  and  $1s^2 2s^2 2p^6 3s^2 3p^2 3d^0 4f^0$ , respectively, where d and f orbitals are introduced to increase transferability of the pseudopotentials. Cutoff radii for the atomic orbitals are taken to be as small as possible to enhance transferability as well as to enable atomistic calculations at shorter interatomic separations as precisely as possible. The smallest cutoff radius for atomic orbitals in pseudopotential generation methods is restricted by the length at which the outermost nodes of the orbitals are formed in an all-electron calculation. In this work all-electron calculations show that 3s and 3p orbitals form outermost nodes near 0.7 a.u. for Si [ $1s^2 2s^2 2p^6 3s^2 3p^2$ ] and 0.5 a.u. for Ar [ $1s^2 2s^2 2p^6 3s^2 3p^6$ ], as depicted in Fig. 1. Orbital cutoff distances must be larger than these values to avoid creation of ghost states in the SIESTA self-consistent calculations. The smallest cutoff distance for Si is found to be 1.20 a.u. for 3p orbitals, while cutoffs can be taken as small as 1.1 a.u. for s, d and f orbitals. The smallest possible cutoff for Ar is found to be around 0.8 a.u. The pseudopotentials generated here are validated against energy levels and logarithmic derivatives from all electron calculations. Energy levels are found to differ by less than 1 mRy for different electronic configurations and computed logarithmic derivatives at distances larger than the cutoff radii show good agreement with the all electron calculations.

The basis set used here relies on the Sankey type localized pseudoatomic orbitals (PAOs) that include multiple-zeta decays. The exchange and correlations are treated with the local density approximation and the parameterization of Ceperly and Alder [30]. For all calculations, an energy shift of 20 meV and a split norm of 0.15 are found to be sufficient to converge the basis set.

To compute two-body interaction energies between two atoms, Ar and Si are put in a box, large enough for the wavefunctions to have negligible interactions with their periodic images and the calculations are performed with different interatomic distances ranging from 0.4 to 3.0 Å. To achieve convergence a large mesh cutoff of 300 Ry and a sufficiently dense  $20 \times 20 \times 20$  Monkhorst-Pack real space grid is used in the self-consistent calculations. Finally, a tolerance of 0.1 mRy is used for convergence of the total energy for each interatomic distance.

The interaction potential is extracted by subtracting free energies of the atoms from total energies using the relation:  $E_{\text{Ar-Si}} = E_{\text{Ar-Si in supercell}} - E_{\text{Ar}} - E_{\text{Si}}$ , where  $E_i$  ( $i = \text{Si, Ar}$ ) is the atomic free energy. The free energies are calculated by putting each atom separately in a large box and taking the spins as polarized. The total

energy has five components: Hartree energy, exchange-correlation energy, ion-ion repulsive energy, ion-electron attractive energy and electron kinetic energy. As the atoms approach, changes in interaction energy become significant for interatomic distances of less than 2.0 Å. For a distance of less than 2.0 Å all of the energies increase with a reduction in interatomic separation but the change in individual energies occurs at different scales. Ion-ion repulsive energy changes exponentially and dominates the total energy change at such shorter distances.

Based on the results of this energy analysis, interaction potentials are fitted to the same functional forms used for both the Molire and ZBL potentials:

$$V(r) = \frac{Z_1 Z_2}{r} \sum_{i=1}^n \alpha_i e^{-\beta_i r/a}, \quad (1)$$

$$a = 0.4683(Z_1^{2/3} + Z_2^{2/3})^{-3/2}, \quad (2)$$

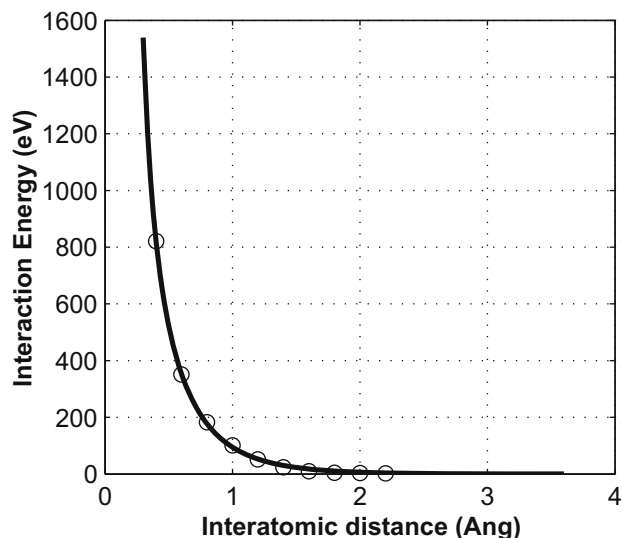


**Fig. 2.** Two-body interaction potential using DFT. Open circles show the data points obtained with DFT and the solid line represents the nonlinear least-square fitted potential function.

**Table 1**  
Parameters for three different potentials.

	DFT-ArSi	Molire	ZBL
$\alpha_1$	0.196158	0.35	0.18180
$\alpha_2$	1.367985	0.55	0.50990
$\alpha_3$	4.512625	0.10	0.28020
$\alpha_4$	0.00	0.0	0.02817
$\beta_1$	0.257385	0.30	3.20
$\beta_2$	2.322177	1.20	0.94230
$\beta_3$	2.446491	6.00	0.40290
$\beta_4$	0	0	0.20160

**Table 2**

The parameters for screening length used in different models. Parameters obtained with DFT-ArSi data are closer to ZBL parameters. The Molire potential uses either Lindhard or Firsov's expressions of screening length.

	$\gamma_1$	$\gamma_2$	$\gamma_3$
DFT-ArSi	0.22	0.22	1.0
ZBL	0.23	0.23	1.0
Lindhard	2/3	2/3	1/2
Firsov	1/2	1/2	2/3

where  $n = 3$  for Moliere and DFT-ArSi and  $n = 4$  for ZBL,  $Z_i$  is the atomic number of interacting atoms,  $\alpha_i$ ,  $\beta_i$  and  $\gamma_i$  are fitting constants,  $r$  is the interatomic separation and  $a$  is the screening length. A standard least-square fit is used to calculate these parameters. Both the DFT-ArSi data and the fitted functions are plotted in Fig. 2. The best fit parameters along with the parameters of ZBL and Moliere are listed in Table 1. The screening length parameters are tabulated separately and compared with other available parameters in Table 2.

The three different potential energy functions are plotted in Fig. 3 on a semilogarithmic scale. The ZBL potential energy is less than the Moliere potential energy for all values of  $r$  while the DFT-ArSi potential is less than the Moliere potential within 1 Å and less than the ZBL potential within 0.6 Å. The corresponding forces are shown in Fig. 4. The DFT-ArSi force is greatest within a distance of  $\sim 0.5$  Å.

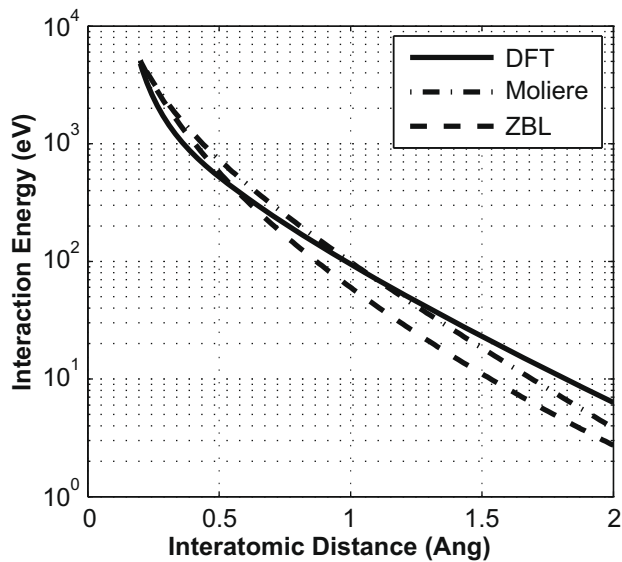


Fig. 3. Comparison of the DFT-ArSi potential with that of Moliere and ZBL. The DFT-ArSi potential is found to be intermediate relative to the other two for the most important range of interatomic separation for keV ion bombardment, 0.5–1.0 Å.

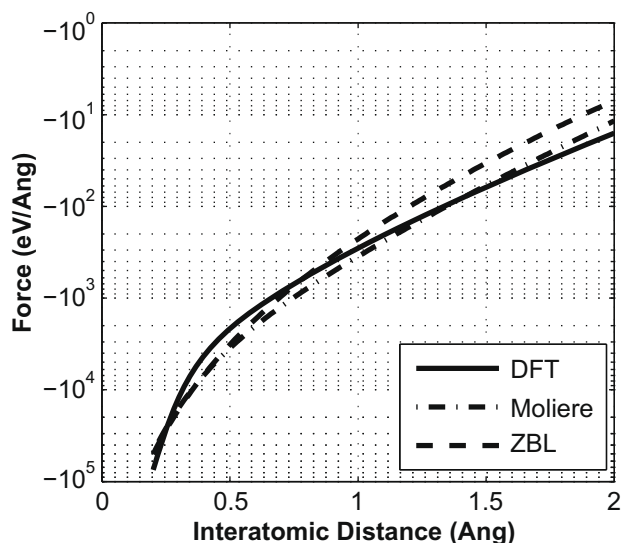


Fig. 4. Comparison of force functions obtained by taking derivatives of the potential functions.

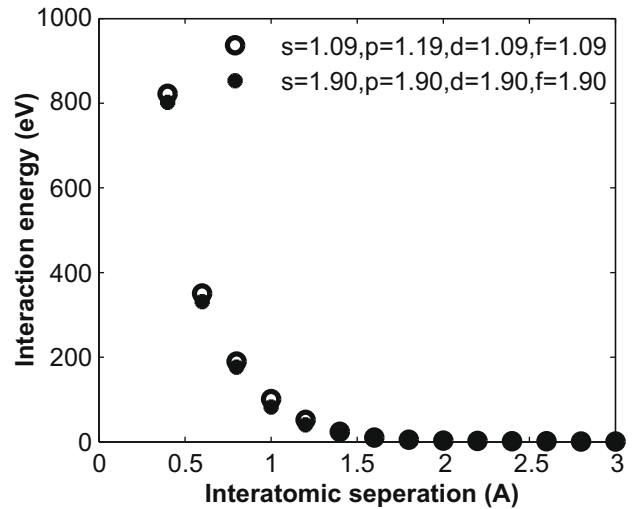


Fig. 5. Effect of cutoff radius on the interaction potential.

The smallest distance at which the DFT-ArSi fitting is carried out is 0.76 a.u., which is smaller than the sum of the smallest cutoff radii for the Ar–Si atom pair. This is justified by comparing the computed interaction energy obtained using the smallest possible cutoff radii,  $r_c^{\text{smallest}} = 1.10(\text{Si}), 0.70(\text{Ar})$  a.u., to that for larger cutoffs,  $r_c^{\text{smallest}} = 1.90(\text{Si}), 3.05(\text{Ar})$  a.u. As shown in Fig. 5, energies obtained in this way differ by less than 2% at small separations.

To identify possible effects of the presence of neighbors the two-body interaction energies are recalculated with the Si belonging to a bulk-like environment. In this case, a supercell is constructed with 64 Si atoms and one Ar atom. Lattice vectors are chosen such that the supercell is periodic only in the [100] and [010] directions. The Ar atom is placed near the [001] surface atoms and the lattice vector in the [001] direction is taken to be large enough that Ar interactions with the image of the supercell are negligible. A  $4 \times 4 \times 2$  Monkhorst-Pack energy grid is found to be sufficient for convergence. The Ar atom position is varied along the surface normal and energies are computed as a function of distance between Ar and Si using the relation:  $E_{\text{interaction}} = E_{\text{supercell}} - E_{\text{Ar}} - 64 \times E_{\text{Si}}$  Figs. 6 and 7 compare the interaction energies and forces obtained when treating Si as a free atom or as belonging to bulk. The energy difference is negligible compared

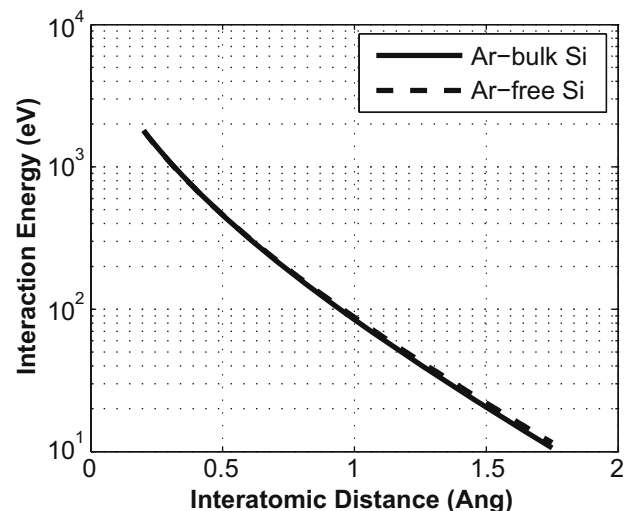


Fig. 6. Effect of neighbors on the two-body interaction potential.

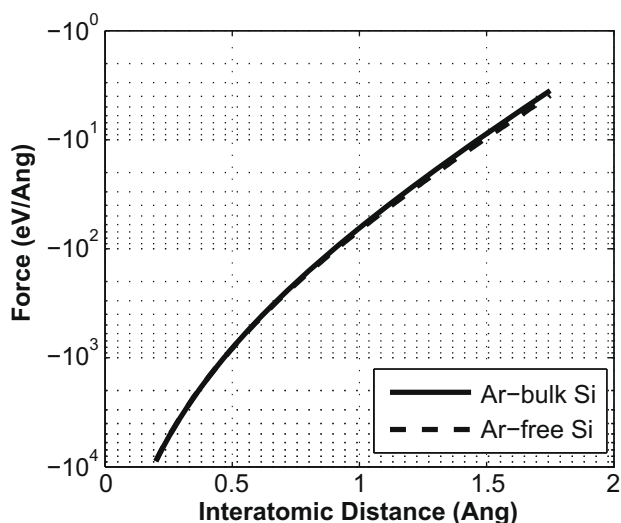


Fig. 7. Effect of neighbors on the two-body interaction force.

to the energy of the incident particle when the distance between interacting Ar–Si atom pairs is less than 1.0 Å.

Sputter yield molecular dynamics calculations are then carried out using this DFT–ArSi empirical potential based on the first-principles results and the Moliere potential for direct comparison. To focus on exclusively on the effects of the Ar–Si potential in the computed sputter yield, sputter yield results are compared to other available computational results that are obtained with the SW potential for Si–Si interactions, but with different repulsive potentials for the Ar–Si interactions. A comprehensive comparison with many results from the literature, including results from the popular SRIM-2008 code which uses a Monte-Carlo technique, is presented in the next section.

### 3. Results and discussion

The DFT–ArSi calculated Si sputter yield is 0.59 at 500 eV and 0.90 at 1 keV. Since different values for experimental sputter yields are observed in the literature arithmetic averages of the most recent experimental measurements, presented in Table 3, are used to benchmark these results. Errors are computed as the relative difference of the computational values with the experimental values and are shown in Table 3 as percentages. The average experimental sputter yield is 0.63 for 500 eV and 0.88 for 1 keV. Hence, the DFT–ArSi results are only 6.3% low for 500 eV and 2.3% high for 1 keV ion impacts. This is a significant improvement in the predicted

sputter yield compared with that obtained by any other potential, as seen in Table 3. The ZBL potential is found to be closer to the experimental values than any potential other than the DFT–ArSi potential, with errors of +11% at 1 keV and –11% at 500 eV. Except for the SRIM-2008 results, all the other computational studies involve molecular dynamics simulations with the Si–Si interactions described by Stillinger–Weber potential.

It is interesting to note that the DFT–ArSi and the ZBL potentials result in sputter yields higher than the experimental values at 1 keV and lower than the experimental values at 500 eV. The ZBL potential is a universal potential and not specific to the Ar–Si system. The SCF potential is developed with using the  $\text{SiH}_3\text{Ar}^+$  molecule, ignoring correlation effects and including two d-polarization functions in a Gaussian basis. The convergence of this potential with respect to the assumed triple-zeta basis or orbitals is not reported in the literature. Furthermore, no justification is made for modeling the Ar–Si interaction using  $\text{SiH}_3\text{Ar}^+$  instead of  $\text{Si}_3\text{Ar}^+$  and the effect of second neighbors is completely ignored, which is shown in Fig. 6 to be potentially important for interaction distances larger than 1 Å. The SCF potential gives yields significantly higher than experimental values for both energies considered. The authors attribute these differences to surface reconstruction, yet these reconstructions should vanish at very small fluence levels. The potential developed by Smith gives very strong interactions at all interatomic distances and gives rise to higher sputter yields compared to any other potential. On the other hand, the Moliere potential and the SRIM code give lower yields for all the energies considered here or reported in the literature. The error is more significant at energies below 1 keV [6,23,37]. Wittmaack [1] analyze the reliability of SRIM results and show that yields computed by SRIM are much less than experimental values when the atomic number of the projectile atom is smaller than that of the target atom, i.e.  $Z_1/Z_2 < 1.0$ .

At lower incidence energies most computed results (i.e. DFT–ArSi, Moliere, SRIM) deviate from the experimental measurements more significantly. Although DFT–ArSi gives the closest match to the experimental measurements and sputter yields are found to vary in a consistent way, the computed value at low energy is still seen to deviate by 6%. It is difficult to accurately compute sputter yields for the lowest energies because the long-range tail of the ion–solid interaction potential is more significant relative to the kinetic energy of the ion. Based on our results the Stillinger–Weber potential is sufficiently accurate for modeling Si–Si interactions. Our results suggest, however, that at the lowest incidence energies, for the 1.5 Å separation range, the details of the long range tail of the Ar–Si interaction become more important; this is evidently due to the details of the electronic structure rather than the model of the target material or structure.

Table 3

Sputtering yield at 500 eV and 1 keV Ar impact energies.

	500 eV		1 keV	
	SY	% Error	SY	% Error
Expt.	0.63 <sup>a</sup>	–	0.88 <sup>b</sup>	–
DFT–ArSi	0.59 <sup>c</sup>	–6.3	0.90 <sup>c</sup>	+2.3
ZBL	0.56	–11.1	0.98	+11.4
SDCI/SCF	0.70	+11.1	1.10	+25.0
Smith	0.84	+33.3	1.33	+51.1
Moliere	0.47 <sup>d</sup>	–25.4	0.84 <sup>c</sup>	–4.5
SRIM-2008	0.28 <sup>c</sup>	–55.6	0.74 <sup>e</sup>	–15.9

<sup>p</sup> [2], <sup>q</sup> [31], <sup>r</sup> [32], <sup>s</sup> [33], <sup>t</sup> [34], <sup>u</sup> [35], <sup>v</sup> [22], <sup>w</sup> [36], <sup>x</sup> [6].

<sup>a</sup> Average of (0.68<sup>p</sup>, 0.63<sup>q</sup>, 0.61<sup>r</sup>, 0.60<sup>s</sup>).

<sup>b</sup> Average of (0.93<sup>p</sup>, 0.90<sup>q</sup>, 0.80<sup>u</sup>).

<sup>c</sup> This work.

<sup>d</sup> Average of (0.46<sup>c</sup>, 0.45<sup>v</sup>, 0.49<sup>w</sup>).

<sup>e</sup> Average of (0.76<sup>c</sup>, 0.72<sup>x</sup>).

### 4. Conclusion

In summary, computed sputter yields using the DFT–ArSi potential for both 500 eV and 1 keV incidence energies show better agreement with experimental data than results obtained using other available potentials. The DFT–ArSi potential is derived specifically for Ar–Si interactions using a first-principles electronic structure approach. The potential is found to give larger interaction energy compared to other available potentials at an interatomic separation distance of more than  $\sim 1.5$  Å. This appears to be an important length scale for describing ion–target interactions in lower energy ion–bombardment. While the use of the SW potential for the target material may introduce some error for modeling ion bombardment, especially at lower energies, the use of the new potential eliminates most of the error associated with sputter yield predictions using other Ar–Si potentials, even when the SW

potential is used for Si–Si interactions. The use of the new potential may lead to better a physical understanding of some ion-bombardment related problems.

### Acknowledgement

The authors thank Prof. Richard M. Martin and Prof. Todd J. Martinez for many helpful discussions. The generous support of NSF Grant CMS-05-10624 is gratefully acknowledged.

### References

- [1] K. Wittmaack, Phys. Rev. B 68 (2003) 235211.
- [2] P.C. Zalm, J. Appl. Phys. 54 (1983) 2660.
- [3] R.A. Stansfield, K. Broomfield, D.C. Clary, Phys. Rev. B 39 (1989) 7680.
- [4] G. Molière, Z. Naturforsch. 2a (1947) 133.
- [5] J.F. Ziegler, J.P. Biersack, U. Littmark, *The Stopping and Range of Ions in Solids*, Pergamon, New York, 1985.
- [6] <[www.srim.org](http://www.srim.org)>, A Monte-Carlo Computer Program to Calculate Sputter Yields.
- [7] V.I. Shulga, Nucl. Instr. and Meth. B 254 (2007) 200.
- [8] A. Akkerman, J. Barak, IEEE Trans. Nucl. Sci. 53 (2006) 3667.
- [9] D.E. Harrison Jr., J. Appl. Phys. 52 (1981) 1499.
- [10] R.P. Webb, D.E. Harrison Jr., J. Appl. Phys. 53 (1982) 4193.
- [11] M.H. Shapiro, P. Lu, Nucl. Instr. and Meth. B 215 (2004) 326.
- [12] A. Schüller, G. Adamov, S. Wethekam, K. Maass, A. Mertens, H. Winter, Phys. Rev. A 69 (2004) 050901.
- [13] A.J. García, J.E. Miraglia, Phys. Rev. A 74 (2006) 012902.
- [14] K. Nordlund, N. Runeberg, D. Sundholm, Nucl. Instr. and Meth. B 132 (1997) 45.
- [15] K. Broomfield, R.A. Stansfield, D.C. Clary, Surf. Sci. 202 (1988) 320.
- [16] A.J. García, J.E. Miraglia, Phys. Rev. A 75 (2007) 042904.
- [17] H. Ohta, S. Hamaguchi, J. Chem. Phys. 115 (2001) 6679.
- [18] M. Taguchi, S. Hamaguchi, J. Appl. Phys. 100 (2006) 123305.
- [19] L.E. Carter, S. Khodabandeh, P.C. Weakliem, E.A. Carter, J. Chem. Phys. 100 (1994) 2277.
- [20] D.E. Hanson, A.F. Voter, J.D. Kress, J. Chem. Phys. 110 (1999) 5983.
- [21] C.F. Abrams, D.B. Graves, J. Vac. Sci. Technol. A 16 (1998) 3006.
- [22] P. Hohenberg, W. Kohn, Phys. Rev. 136 (1964) 864.
- [23] M.C. Moore, N. Kalyanasundaram, J.B. Freund, H.T. Johnson, Nucl. Instr. and Meth. B 225 (2004) 241.
- [24] M.Z. Hossain, J.B. Freund, H.T. Johnson, J. Appl. Phys. 103 (2008) 073508.
- [25] R.J. MacDonald, Rad. Eff. 3 (1970) 131.
- [26] H.H. Andersen, H.L. Bay, in: R. Behrisch (Ed.), *Sputtering by Particle Bombardment I*, Springer-Verlag, Berlin, 1981, p. 145.
- [27] F.H. Stillinger, T.A. Weber, Phys. Rev. B 31 (1985) 5262.
- [28] J.M. Soler, E. Artacho, J.D. Gale, A. García, J. Junquera, P. Ordejón, D. Sánchez-Portal, J. Phys.: Condens. Matter 14 (2002) 2745.
- [29] N. Troullier, J.L. Martins, Phys. Rev. B 43 (1991) 1993.
- [30] D.M. Ceperley, B.J. Alder, Phys. Rev. Lett. 45 (1980) 566.
- [31] J.M.E. Harper, J.J. Cuomo, P.A. Leary, G.M. Summa, H.R. Kaufmann, F.J. Bresnock, J. Electrochem. Soc. 128 (1981) 1077.
- [32] C. Steinbrüchel, Appl. Phys. Lett. 55 (1989) 1960.
- [33] P.C. Zalm, L.J. Beckers, F.H.M. Sanders, Nucl. Instr. and Meth. B 209 (1983) 561.
- [34] U. Gerlach-Meyer, J.W. Coburn, E. Kay, Surf. Sci. 103 (1981) 177.
- [35] D.J. Oostra, R.P. van Ingen, A. Haring, A.E. de Vries, G.N.A. van Veen, Appl. Phys. Lett. 50 (1987) 1506.
- [36] E.F.C. Haddeman, B.J. Thijsse, Nucl. Instr. and Meth. B 202 (2003) 161.
- [37] K. Wittmaack, J. Appl. Phys. 96 (2004) 2632.